Automated finite element modeling of a human mandible with dental implants

Stefan Fütterling[1], Reinhard Klein[1], Wolfgang Straßer[1], Heiner Weber[2]

[1]Universität Tübingen, Wilhelm-Schickard-Institut für Informatik, Graphisch Interaktive Systeme (WSI-GRIS), Auf der Morgenstelle 10C, 72076 Tübingen, Email: stefan@gris.uni-tuebingen.de

[2]Zentrum für Zahn-, Mund- und Kieferheilkunde, Poliklinik für zahnärztliche Prothetik, Osianderstr. 2-8, 72074 Tübingen, Germany

Abstract

This paper presents an automated procedure to generate a three-dimensional finite element model of an individual patient's mandible with dental implants inserted. The reconstruction of the geometry as well as the modeling of the material properties for the different types of bone in the jaw is based on CT data.

For this purpose various methods of image processing, geometric modeling and finite element analysis are combined and extended. Special emphasis is given to the automated assignment of the material properties based on the density values of the CT data, a technique that replaces the geometric modeling of the inner structures of the bone and makes it possible to run the generation process of the model in an automated way.

Finally we focus on a comparison of a mandible with different material modeling strategies that shows the quality of the finite element models.

1 Introduction

Stress transmitted to the bone around osseointegrated implants can cause reabsorption of the bone and other biomechanical remodeling processes, that can end in the loss of the implants. Structural analysis using the finite element method is becoming very common in computer aided surgery planning (CAS), but building a finite element model of individual patients' bones and implants is a costly process.

Our intention was to develop an automated procedure for the reconstruction of the individual patients' bone geometry on the basis of computer tomography (CT) data and a tool for the surgeons to place implants into the bone interactively. These geometry models are then converted to finite element models using adaptive tetrahedral meshing.

Besides the exact geometric modeling, the material properties given to the bone have a major impact on the analysis results. For technical parts and materials, for instance in mechanical engineering, the material properties and the geometry are well defined. In biomechanical structures like the human mandible however, the type of bone as well as the density are changing strongly throughout the geometry, thus averaging and assignment of only one or two material properties can lead to inaccurate results.

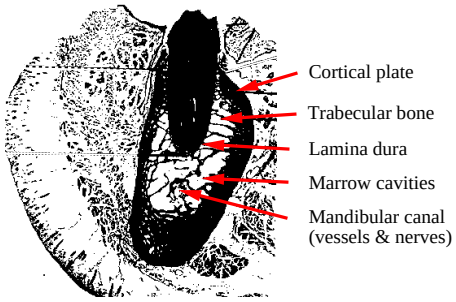

Figure 1: Buccolingual section of the mandible

Figure 1 shows the two main bone types of the mandible, the hard cortical plate that forms the shell of the jaw, and the trabecular (spongy, cancellous) bone inside. The thickness of the corticalis and the consistency of the spongiosa vary strongly throughout the mandible. The trabecular bone is composed of plate-like bone partitions with bone marrow spaces of various sizes and shapes and contains the mandibular canal for the inferior alveolar vessels and nerves and other cavities [Woelf79]. An exact border between the cortical and cancellous bone cannot be determined.

For these reasons we define a range of seven bone material properties from very soft cancellous bone to hard cortical bone. These are then assigned to to the elements of the mandible finite element mesh depending on the density values in the patient's CT data. The analysis results are then compared to finite element models with only one material defined for the entire bone.

The advantages of this automated geometry and material modeling system are better implantation planning tools, enhanced positioning, design and longevity of the implants, minimization of the stresses induced into the bone and thus prevention of damage or loss of the implants.

2 Previous work

Several authors published finite element studies of human bones with osseointegrated implants or prostheses systems, for example dental implants in the mandible or femoral implants. They are mostly concentrating on the implant design, the bone-implant interface and the stresses induced into the bone. The following descriptions focus on mandible models with endosseous dental implants.

Some of the studies are confined to a small area or volume of bone around the implants. They use either two-dimensional scenarios of implants placed into a rectangular area of bone assuming symmetry [Siege93] or three-dimensional implant models placed into a rectangular volume of bone. Material definitions are then made for two bone materials, a layer of cortical bone covering the inner trabecular bone.

The analysis focuses on the minimization of the stresses and strains in the implant-bone interface that result to different loads by testing different implant materials and shapes. These studies are confined to a small volume of bone around the implant and two material properties. They do not investigate the impacts of the implant on the entire bone structure and they assume an exact border between the two materials.

Other analysis studies use complete three-dimensional models of bones, for instance a human mandible. The geometry of these models was either idealized and created with a CAD system [Borus96, Kregz93], reconstructed from CT scans [Hart92] or from a real mandible specimen that was cut into slices [Meije93]. Two of these three-dimensional models [Hart92, Meije93] model the border of the cortical plate and assign different material properties for cortical and cancellous bone, the others use average bone materials for the whole jaw model.

None of the authors published an automated procedure to reconstruct the individual bone geometry of a patient's mandible and they assigned a maximum number of two different material definitions for cortical and trabecular bone, assuming a distinguished border of the cortical plate.

3 Data acquisition

The geometry and material data are acquired from CT-slices of the patient. The maximum available spatial resolution within a slice is about 0.5 mm and about 1 mm between two slices. In order to minimize the radiation for the patient, in most real data-sets the distance between two layers is greater. Typical resolutions of the 2D-Slices are 256×256, 512×512 or 1024×1024. Each pixel possesses an information depth of either 12 Bit (4096 grey values) or 16 Bit (65536 grey values). The data are given in the DICOM format and can be read into the Tübinger Med-Station, an interface for medical diagnosis and therapy on all different kinds of digital medical image data [Grune95]. The Med-Station offers different kinds of 2D and 3D filter operations for viewing and for the segmentation of the data-set.

4 Segmentation

The segmentation of the mandible from the CT data-set is done using the automatic digital image segmentation tool implemented in the Med-Station [Grune95]. This tool uses a threshold technique to detect edges automatically. It works fine for the outer shape of the mandible, because its density in the grey values differs significantly from the surrounding tissue.

If the CT-data contain major artifacts, e.g if some of teeth have fillings, or if the mandible is in contact with other bones in the region of the temporo-mandibular joint, the contours of the mandible cannot be detected properly and user interaction is necessary. Our tool then gives the possibility to select and modify the contours or to insert additional contours using a method that is based on the intelligent scissors proposed by Mortensen and Barrett [Morte95]. When the gestured mouse position comes in proximity to an edge of the mandible, a live-wire boundary snaps to, and wraps around the object of interest.

As a result of the 2D-segmentation we get a stack of bitmaps that are used as input data for the reconstruction of the mandible shape.

Figure 2: CT slice of a mandible

As you ca see in Figure 2, it is not possible to reliably detect any border between the cortical plate and the cancellous inner region of the mandible without massive interaction of a medically skilled user. In our tests, various users chose different border contours for the cortical plate, and these often resulted in bad geometries after the reconstruction over several slices. The main disadvantage however was the time-consuming interactive editing of the inner contours.
On the other hand, the trabecular regions of the mandible contain areas of higher and lower densities and the mandibular canal, that cannot be modeled in the required level of detail.

For these reasons we decided to just segment the outer shape of the mandible and to solve the problem

of the different types and regions inside the jaw by assigning different material properties to the tetrahedral finite elements depending on the density grey values in the CT data-set. An exact geometric modeling of the cortical and cancellous zones inside the jaw bone can thus be omitted.

5 Reconstruction

The reconstruction of the mandible geometry from the bitmap stack is done by a marching cubes algorithm [Liebi96]. The result is a closed triangle mesh that represents the shape of the jaw bone.

Because these surface triangle meshes contain several thousand small triangles, a mesh simplification is done to reduce the number of triangles. We use a multi-resolution model for the reduction, in order to be able to re-insert the small triangles at the locations where the implants are inserted into the mandible.

5.1 The marching cubes algorithm

The output triangle mesh of the mandible must define a closed 2-manifold in order to represent a volume and allow for 3D-meshing. This implies that no vertex of the triangle mesh is complex and each edge of the triangle mesh belongs to exactly two triangles. In its original version the Marching Cubes algorithm only produces a set of triangles without neighborhood information and it does not take care of this special topological requirements. The output triangle set contains complex vertices as well as edges that share more than two triangles. Such cases occur if one or more intersection points between the edges of a cube and the object are equal to a vertex p_{ijk} of the cube. This is the case if the grey-values $f(p_{ijk}) = c$, where c is the threshold value. In this cases triangles as they are stored in the look-up tables of the marching cubes algorithm degenerate to edges or vertices. This is shown in Figure 3.

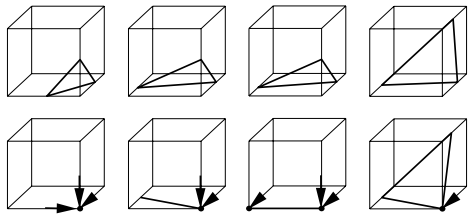

Figure 3: Degeneration of triangles at cube corners.

5.1.1 Anti-grid-snapping

The idea of the anti-grid-snapping avoids the generation of non-manifold triangle meshes in the marching cubes algorithm. It is based on the following observation: *If none of the gray-values $f(p_{ijk})$ of the vertices considered by the marching cubes algorithm is equal to the threshold value c the marching cubes algorithm generates a 2-manifold triangle mesh.* Therefore, if we detect a vertex p_{ijk} with $f(p_{ijk}) = c$ the threshold value c is a little bit changed but the classification of the vertex remains the same. In such a way all intersection vertices belong to the inner of the edges of the cubes and the output of the algorithm is always a 2-manifold mesh. For the changes of the threshold values in practice we use the values k_{anti} and $1 - k_{anti}$ instead of 0 and 1 performing the linear interpolation to define the intersection vertex between the actual surface and an edge of a cube.

5.1.2 Generating the connectivity

In the following steps aside from the geometry of the mesh, also its connectivity is of interest. The connectivity of a triangle mesh comprehends all adjacency relationships of the mesh. To establish the connectivity of the resulting mesh we note that all inner edges of the volume data-set belong to four cubes and it is enough to compute the intersection vertex between the surface and an edge only once. If the volume data-set is processed in sequential order this can easily be done: in each marching step of the algorithm only three of the twelve edges have to be considered. The other nine edges belong to an already processed cube:

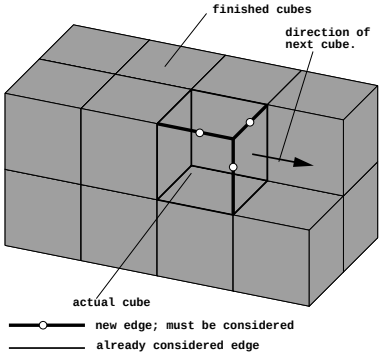

Figure 4: In each marching step only on three edges intersection points must be computed.

If a new intersection vertex is found on an edge it is stored in a vertex array and its position pos_{index} in the vertex array is stored in a pair $((i, j, k), pos_{index})$, where (i, j, k) is the identifier of the edge. To avoid the allocation of unnecessary storage only those pairs are stored for which an intersection is found. For fast relocation of a pair a binary search tree is used.

5.1.3 Inner mandible structures

Depending on the inner bone densities and the chosen threshold value, the marching cubes algorithm also reconstructs the shape of the inner cancellous structures of the jaw.

Because these inner meshes are very fine and complicated and introduce problems to the automated geometry modeling process, we decided to use the ver-

tices of these inner meshes as additional mesh seeds for the finite element tet-mesher. Because these Steiner vertices represent locations of a high grey value gradient in the CT data-set, the resulting finite element tetrahedron boundaries are most adapted to the geometrical structures inside the mandible and thus optimized for later material properties assignment.

5.2 Mesh simplification

One of the major drawbacks of the original marching cubes algorithm is that due to the given subdivision of space it produces much more triangles than necessary to approximate the boundary surface of the object. Therefore, several enhancements of the original algorithm like adaptive marching cubes [Bloom88] and data reduction by grid snapping [Moore92] where suggested in the literature. Although good reduction rates can be achieved by an adaptive marching cubes algorithm, its implementation is very difficult and therefore error prone [Kloos94].

Therefore, we decided to use only grid-snapping. In this technique intersection vertices on the edges of the cubes with a distance smaller than d_{snap} to a corner vertex of the cube are replaced by the corner vertex itself. The value of d_{snap} is chosen between 0 and 0.5 times the edge length of the cube. In order to avoid the generation of non-manifold triangle meshes the snapping is not performed if multiple edges would be generated. We found, that using grid-snapping depending on the value of d_{snap} reduction rates up to 40% are possible, but the resulting triangle meshes are still very large:

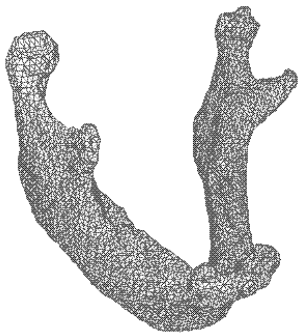

Figure 5: Reconstructed mandible with about 80000 triangles.

Boundary conform 3D-meshing of this surface would result in a FE-mesh that does not allow fast FE-computations. Therefore, the output triangle mesh of the marching cube is converted into a multiresolution model. This model maintains the surface mesh at different levels of detail, where the levels of detail may be different in distinct areas of the object. In such a way the mesh can be refined interactively in the areas of interest, e.g. around the implant, see Figure 6.

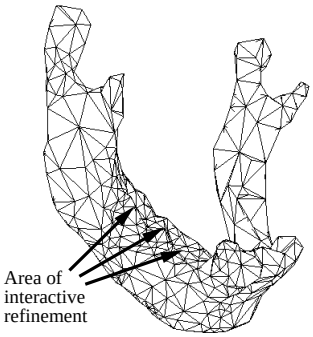

Figure 6: The triangle mesh of the mandible after reduction and selective refinement in the molar area contains only about 900 triangles.

5.3 The simplification algorithm

The simplification algorithm successively simplifies the original triangle mesh Σ_M by removing vertices from the current triangulation. All triangles adjacent to the removed vertex are removed from the current triangulation and the resulting holes are retriangulated. To chose the next vertex for removal, we use the Haussdorff distance between each vertex and the retriangulated area in case of its removal, compared to other authors who use energy criteria [Hoppe93]. This is done until no further vertices can be removed from the simplified triangulation without exceeding a predefined distance between the original triangulation and the simplified one. This is described in detail in [Klein96].

A major problem not considered by the simplification algorithms described in the literature so far is that during the simplification process it may happen that the simplified mesh self intersects. Self intersections occur relatively often while simplifying areas where the mandible is very thin.

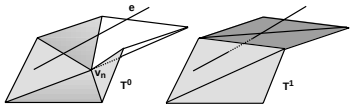

Figure 7: Left: triangle mesh before the removal of vertex v_n. Right: After the removal of v_n, edge *e* intersects the newly generated triangles.

To avoid such self intersections we included an efficient intersection test into our simplification algorithm. This test is based on the following observation, see Figure 7: *Let T^0 be the set of triangles adjacent to vertex v_n and T^1 the triangles forming the retriangulation of the remaining hole after the removal of vertex v_n. Then a self intersection occurs if and only if an edge e intersects a triangle $\Delta \in T^1$.* To perform these test a regular grid structure is used. Each grid cell contains all edges of the current triangulation intersecting the cell. To keep this data structure consistent in each simplification step the inner edges of the removed tri-

angles are deleted from and the new edges are inserted into the grid structure. To insert into and delete edges from the regular grid a modified 3D-DDA-algorithm is used.

Using this grid structure only the edges contained in bounding box of each new triangle with respect to the grid have to be considered for the intersection test.

5.4 The multiresolution model

From the simplification algorithm a multiresolution model can be generated:

- A sequence of the inverse vertex removal operations performed during the simplification algorithm and the coarsest level of detail generated by the simplification algorithm are stored. Then, starting with the coarsest level of detail the original model can be generated by applying the stored operations in reverse order. If in addition not only refinement operations but also coarsening operations should be supported also the vertex remove operations themselves must be stored.
- In addition to the sequence of the vertex remove operations and their inverse operations dependencies are necessary. These dependencies store the information needed to determine for each vertex remove operation or its inverse which triangles must be present in the current triangle mesh before the operation can be performed.

We use an interactive multiresolution viewer to extract triangle meshes of different levels of detail and to do the refinements at the locations of the implants. The multiresolution model is described in more detail in [Klein97].

6 Implant modeling

The implant modeling package consists of two essential parts, the interactive placement of the implants into the bone and the intersection calculations between the bones and implants.

6.1 The interactive positioning tool

The positioning tool is used to select and interactively place implants into the bone. It has several buttons to move and rotate the implant and four viewports: one isometric viewport that can be manipulated by the user and three viewports for top and side views of the implant position. Several other zoom and viewport options are available and easy to use.

6.2 The intersection algorithm

The geometry of the bone and the positioned implants are directly exported to an intersection calculation routine which performs the Boolean operations. This program determines the surface mesh that represents the

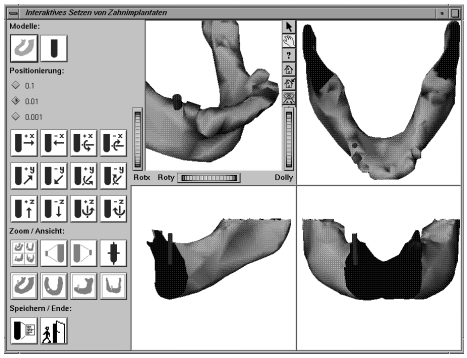

Figure 8: Interactive positioning of an dental implant into the mandible bone

bone with the holes where the implants fits into. Additionally, the implant is modified so that its edges and its faces are identical to the edges and faces of the hole in the bone. This is necessary for the generation of consistent finite element models.

We use the following algorithm for the efficient realization of Boolean operations between two closed triangular surface meshes:

- Determine all triangles of the bone geometry that have an intersection with the implant and calculate the resulting intersections. To accelerate these calculations we use a plane sweep algorithm for the bounding boxes of the triangles. But also a regular grid structure may perform well for this purpose.
- Insert all intersection points and edges into the two intersected triangle meshes. The main operation in this step is to insert vertices and edges into the triangles and to compute a regular retriangulation of the triangles.

After this computations the result of different Boolean operations can be computed easily by establishing new neighborhoods between every four triangles incident to an intersection edge.

6.3 Improvement of the intersected meshes

After the Boolean operation the resulting triangle meshes contain very small triangles and triangles with bad aspect ratios, see Figure 9. For FE-computation such triangles must be eliminated. For this purpose the following steps are performed:

- Remove vertices that are close to the intersection polygon generated during the Boolean operation. In such a way triangles which are to small are avoided.
- Optimize the resulting mesh by inserting Steiner vertices.

To optimize the resulting mesh we use a modification of the refinement algorithm proposed by Chew [Chew93]. This algorithm enhances the idea of the Delaunay triangulation to 2D-surfaces embedded in 3D.

The usage of this algorithm ensures that none of the angles of the triangles in the resulting Steiner triangulation is smaller than 30°:

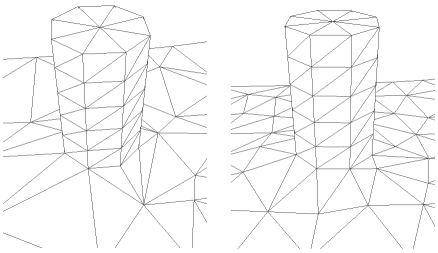

Figure 9: Left: After intersection, the resulting mesh contains small triangles and triangles with bad aspect ratio. Right: After inserting Steiner vertices.

7 Finite element analysis

A series of finite element computations have been performed with a mandible model containing two molar implants to verify the quality of the models obtained by our automated modeling process and to simulate the stresses induced to the bone under typical chewing conditions. Special emphasis is given to a comparison of the results of our automated material properties assignment to a mandible model having only one material property defined.

Three steps are required to build a finite element model based on the surface triangle meshes of the mandible and the implants: 3D-meshing with tetrahedral finite elements, material properties modeling and definition of the load cases. These steps are performed using the commercial finite element preprocessing system PATRAN, numerical solving is done by ABAQUS, and results postprocessing and visualization is again performed in PATRAN.

7.1 Finite element meshing

After conversion from our own geometry representation format to the PATRAN neutral file format, the surface mesh data of the mandible and the implants are imported to the preprocessor. The volumes of the mandible and implants are then meshed with second order tetrahedrons (Tet10), which have ten nodes (four corner and additional six edge nodes) and produce more accurate analysis results than first order tetras.

Because we use smaller triangles in the mandible surface model and additional inner Steiner points close to the location of the implants, the PATRAN tetmesher produces a finer finite element mesh automatically in these areas that are of most interest to the structural analysis and a coarser mesh in the other regions of the mandible. The model shown in Figure 11 has 4741 elements.

7.2 Material properties

For the bone material properties we defined a range of seven material definitions from hard cortical properties (bone1) to medium cancellous bone properties (bone5) and soft trabecular bone properties (bone7) for the areas that contain many marrow spaces, the mandibular canal or other cavities. All seven bone materials were assumed to be homogeneous, isotropic and linearly elastic. Although cortical bone is an orthotropic material, this simplification was made for the calculations. Cortical (bone1) and cancellous bone's (bone5) material properties as well as the titanium material properties for the implants are taken from the Biomaterials Properties Database at the University of Michigan [O'Bri96]:

Material properties	Elastic Modulus (GPa)	Density (g/mm^3)	Poisson Ratio
bone1 (cort.)	14.7	0.0013	0.3
bone2	10.0	0.0013	0.3
bone3	5.0	0.0013	0.3
bone4	2.0	0.0013	0.3
bone5 (canc.)	0.5	0.0013	0.3
bone6	0.25	0.0013	0.3
bone7	0.1	0.0013	0.3
titanium	117.0	0.0045	0.33

Table 1: Material properties of bone and titanium

To assign one of these seven material properties to each tetrahedron of the model, we wrote a PATRAN extension that exports the geometry of the tetrahedrons, searches and averages all grey values from the CT data-set contained in the tetrahedron, and assigns the corresponding material property.
Due to the inner Steiner points (see section 5.1.3) the grey values of most of the tetrahedrons are almost homogenious. In this case an average grey value can be computed and the corresponding material assigned. In the other case where the grey values vary strongly throughout the tetrahedron, it must be subdivided further until the homogenious case is achieved. This is again done be inserting additional mesh seeds for the remeshing.
For the two mandible models with only one material property we use for the comparison, we assigned cancellous (bone5) and cortical bone properties (bone1) throughout the jaw.

7.3 Load case

The following set of boundary conditions and loads has been defined for our model:

- Two mastication forces of 80N onto the implants,
- 10 muscle forces of 30N each induced at the angle and lower ramus of the mandible where the masseter muscle inserts,

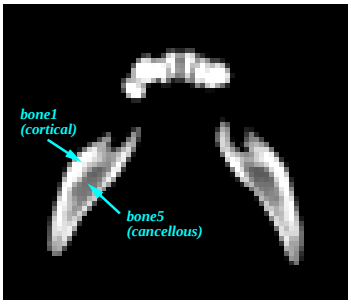

Figure 10: Material properties assignment depending on the density grey values in the CT data-set

- fixed elements in the temporo-mandibular joint.

Figure 11 shows our mandible model with 4741 Tet10 elements and the load case described above:

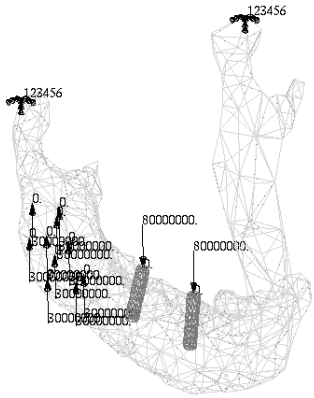

Figure 11: Mandible finite element model with mastication and muscle forces

7.4 Finite element analysis results

The results of the finite element structural analyses for the three models show that the joints and the areas around the implants have the highest resulting stresses induced by the loading.
The implant close to the ramus where the masseter muscle inserts induced high stresses into the surrounding bone. For the model with only cancellous material defined, the highest value of the minor principal stress that can cause reabsorption of the bone was at about -70MPa, a very high value compared to the ultimative compressive strength of bones.
The model with cortical bone material defined for the whole mandible showed significantly lower stresses around the implants. The highest value of the minor principal stress reached about -48MPa.

The model that had the range of seven bone material properties assigned to the tetrahedrons automatically reaches its extreme minor principal stress at about -52MPa, which is between the values of the models having cancellous and cortical material properties assigned throughout. This value is closer to the all-

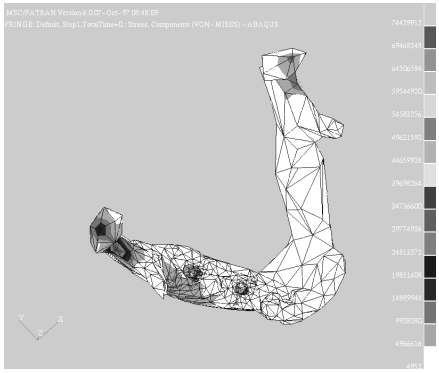

Figure 12: von-Mises average stress induced into the mandible

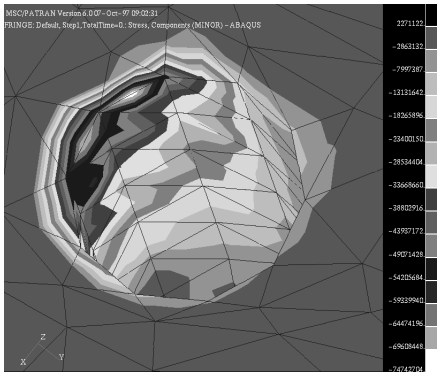

Figure 13: Minor principal stress induced around the implant (cancellous bone material properties)

cortical model, because the location where the implants were inserted contained mostly cortical bone.
The differences in the resulting stresses induced into the bone get greater, if the implant is primarily located in the softer regions inside the mandible, for instance if the patient's cortical plate is not closed at the location where the implants are inserted. This occurs, if the implants are inserted too early after the loss of teeth, or if the jaw already atrophied.

8 Conclusions

The finite elements analysis results show that the chosen methods for the segmentation, the reconstruction of the bone shape and the material properties assignment can be automated for minimum user interaction and result in high quality finite element models. The advanced modeling of the material properties can reduce the amount of geometric modeling to the reconstruction of the bone's shape, using the inner Steiner points delivered by the marching cubes algorithm for optimization of the finite element mesh generation.

References

[Bloom88] J. Bloomenthal. Polygonization of implicit surfaces. *Computer Aided Geometric Design*, 5:341–355,

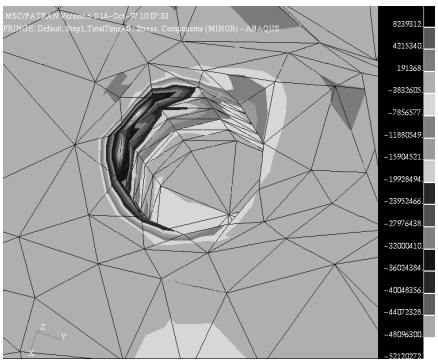

Figure 14: Minor principal stress induced in the area around the implant (automatically assigned range of seven bone material properties)

1988.

[Borus96] Boruszewski, Tortamano, Neto, and Saito. Stress distributions in mandibles around osseo-integrated implants, according to the occlusion pattern, using MSC/NASTRAN three-dimensional modeling. Universidade de São Paulo, Brasil, 1996.

[Chew93] L. P. Chew. Guaranteed-quality mesh generation for curved surfaces. In *Proceedings of the Ninth Annual ACM Symposium on Computational Geometry*, pages 274–280. ACM, ACM Press, 1993.

[Grune95] T. Grunert, J. Fechter, G. Stuhldreier, H.-H. Ehricke, M. Skalej, R. Kolb, and P.E. Huppert. A PACS Workstation with integrated CASE tool and 3D-Endosonography application. In *Computer Assisted Radiology CAR 95*, pages 293–298, 21.-25. June, Berlin, Germany 1995.

[Hart92] R. T. Hart, V. V. Hennebel, N. Thongpreda, W. C. Van Buskirk, and R. C. Anderson. Modeling the biomechanics of the mandible: A three-dimensional finite element study. *Journal of Biomechanics*, 25(3):261–286, 1992.

[Hoppe93] H. Hoppe, T. DeRose, T. Duchamp, J. McDonald, and W. Stuetzle. Mesh Optimization. *Computer Graphics (SIGGRAPH '93 Proceedings)*, vol. 27, pages 19-26, August 1993.

[Klein97] R. Klein and J. Krämer. Multiresolution representations for surface meshes. In *Proceedings of the SCCG (Spring Conference on Computer Graphics), Budmerice, Slovakia*, 1997.

[Klein96] R. Klein, G. Liebich, and W. Straßer. Mesh reduction with error control. In R. Yagel, editor, *Visualization 96*, pages 311–318. ACM, 1996.

[Kloos94] Uwe Kloos. *Graphisch-Interaktive Simulation unter Berücksichtigung medizinischer Fragestellungen*. PhD thesis, Fakultät für Informatik, Universität Tübingen, July 1994.

[Kregz93] M. Kregzde. A method of selecting the best implant prosthesis design option using three-dimensional finite element analysis. *Int. J. of oral and maxillofacial implants*, 8(6):662–673, 1993.

[Liebi96] G. Liebich. *Erzeugung von Oberflächen- und Finite-Elemente-Modellen aus Tomographiedaten*. Master thesis, Fakultät für Informatik, Universität Tübingen, December 1996.

[Loren87] W. E. Lorensen and H. E. Cline. Marching cubes: A high resolution 3D surface construction algorithm. In Maureen C. Stone, editor, *Computer Graphics (SIGGRAPH '87 Proceedings)*, vol. 21, pages 163–169, July 1987.

[Meije93] Meijer, Starmans, Steen, and Bosman. A three-dimensional finite element analysis of bone around dental implants in an edentulous human mandible. *Archs oral Biol.*, 38(6), 1993.

[Moore92] Doug Moore and Joe Warren. Compact isocontours from sampled data. In Paul Heckbert, editor, *Graphics Gems III*, pages 23–28. Acad. Press, Boston, 1992.

[Morte95] Eric N. Mortensen and William A. Barrett. Intelligent scissors for image composition. In Robert Cook, editor, *SIGGRAPH 95 Conference Proceedings*, Annual Conference Series, pages 191–198. ACM SIGGRAPH, 1995.

[O'Bri96] William J. O'Brien. Biomaterials properties database. *http://www.lib.umich.edu/-libhome/Dentistry.lib/Dental_tables/toc.html*, University of Michigan, Quintessence Publishing, 1996.

[Siege93] Siegele and Soltesz. Finite-Elemente- Berechnungen zur Beanspruchung des Kieferknochens um Zahnimplantate. *Zeitschrift für zahnärztliche Implantologie*, 1993.

[Woelf79] Woelfel, Julian B., *Permar's Outline for Dental Anatomy*, Lea and Febiger, Philadelphia 1979.